SCALED VERIFICATION SCENARIOS FOR AGILE AOCS TESTBEDS

R. Geshnizjani, B. Freudenau, W. Fichter
Institute of Flight Mechanics and Control, University of Stuttgart, Pfaffenwaldring 27, 70569 Stuttgart, Germany

Abstract

A scaling procedure is developed to transfer verification scenarios for attitude control algorithms from the specific mission dimensions to the dimensions of ground-based hardware demonstrators. The definition of a dimensionless similarity variable ensures a similar load on control moment gyroscopes actuators in spite of different testbed characteristics such as moment of inertia, wheel angular momentum, and even CMG array architecture.

1. INTRODUCTION

Recent years have seen a rising demand of agility for Earth observation satellites [1] in order to increase both the total number of observations and their distance from the satellite's ground track as illustrated in Figure 1.

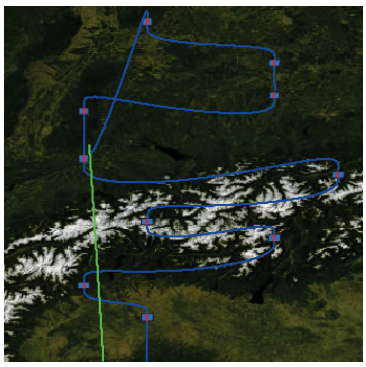

Figure 1 Ground Track (green) and Line of Sight (blue) of Agile Scenario

As the torque requirements of agile missions often exceed the capabilities of conventional reaction wheels, the actuators of choice for agile missions are control moment gyroscopes (CMGs). Using the gyroscopic effect, CMGs act as torque amplification devices, albeit with their own challenges mainly in the form of non-trivial commanding algorithms for the single wheels [2].

Funded by the German Aerospace Agency, the Institute of Flight Mechanics of Control (iFR) cooperates with Airbus Defence and Space in the joint research projects "HOREOS agil" and "HOREOS agad" to develop advanced attitude control algorithms for agile spacecraft with CMGs. In the scope of these projects, a ground-based hardware demonstrator [3] [4] was commissioned at the Airbus site in Immenstaad to verify the developed algorithms in experiments as opposed to pure simulation-based verification campaigns.

Once a ground-based hardware demonstrator exists, its dimensions and dynamical properties (e.g. mass, moment of inertia, actuator capability) are fixed or range in a bounded interval, which may deviate significantly from those of the actual satellite mission of interest. For an experiment to be meaningful, however, the test conditions have to be representative for, i.e. "similar" to, the future application. What "similar" actually means depends on the part of AOCS software that shall be verified.

In this paper, we will first propose some definitions of the term "similar" for different verification goals. Second, for the verification of CMG steering algorithms, we develop a scaling procedure based on the utilization of the CMG array's angular momentum capabilities. To this end, some fundamentals of the attitude control of agile satellites with CMGs are briefly introduced in section 2 followed by a description of the "INTREPID" testbed in section 3. Sections 4 and 5 deal with the scaling of reference scenarios in general and focused on angular momentum utilization, respectively. Finally, section 6 concludes with a case study.

1.1. Nomenclature

H, h	Angular momentum	[Nms]
$\boldsymbol{J}$	Moment of inertia	[kgm²]
$\underline{\boldsymbol{q}}$	Attitude quaternion	[-]
$\boldsymbol{T}$	Rotation matrix	[-]
$\boldsymbol{u}$	Envelope utilization	[-]
β	Skew angle	[rad]
δ	Gimbal angle	[rad]
τ	Torque	[Nm]
ω	Angular rate	[rad/s]

2. ATTITUDE CONTROL OF AGILE SATELLITES

2.1. Control Moment Gyroscopes

A control moment gyroscope (CMG) is an angular momentum exchange device which is composed of a spinning flywheel and a fixed gimbal axis as illustrated by Figure 2.

One challenge of CMG technology is the fact that the orientation of a CMG's angular momentum is not fixed, hence for an *n*-CMG array, the angular momentum at any given time depends on the current gimbal angles $\boldsymbol{\delta} \stackrel{\text{def}}{=} [\delta_1 \quad \cdots \quad \delta_n]^{\mathrm{T}}$ of the CMGs:

(1) $$\boldsymbol{h}_{\mathrm{CMG}} = \sum_{k=1}^{n} \boldsymbol{h}_k(\delta_k)$$

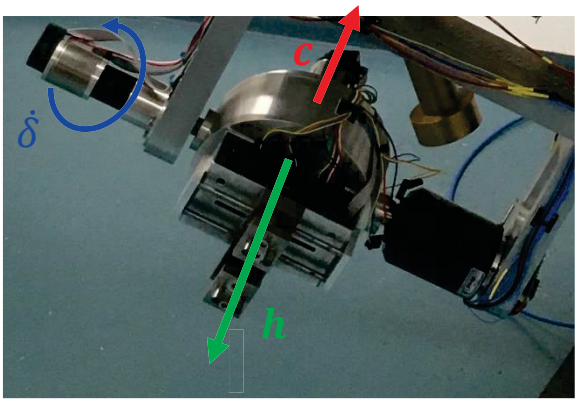

Figure 2 Single Gimbal CMG

The gyroscopic output torque of each CMG acts orthogonal to both its current angular momentum and the gimbal axis, hence the output torque direction of the *k*-th CMG is given by:

$$\boldsymbol{c}_k(\delta_k) = \boldsymbol{g}_k \times \boldsymbol{h}_k(\delta_k)$$

Note that $\boldsymbol{c_k}$ is not a unit vector, but $\|\boldsymbol{c}_k\| = \|\boldsymbol{h}_k\| = h_{\mathrm{fw}}$, where h_{fw} denotes the magnitude of the CMG flywheel's angular momentum and is assumed constant and equal for all CMGs. Defining the Jacobian as $\boldsymbol{C}(\boldsymbol{\delta}) = [\boldsymbol{c}_1 \ \cdots \ \boldsymbol{c}_n]$, the output torque of a CMG array is given by:

(2) $$\dot{\boldsymbol{h}}_{\mathrm{CMG}} = \sum_{k=1}^{n} \boldsymbol{c}_k(\delta_k)\,\dot{\delta}_k = \boldsymbol{C}(\boldsymbol{\delta})\dot{\boldsymbol{\delta}}$$

A more detailed study of CMG dynamics can be found in e.g. [5], [2], and [6].

2.2. Attitude Control Architecture

For a spacecraft with CMGs, the total angular momentum is given by

(3) $$\boldsymbol{H}_{\mathrm{tot}} = \boldsymbol{J}\boldsymbol{\omega} + \boldsymbol{h}_{\mathrm{CMG}},$$

where $\boldsymbol{J}$ is the moment of inertia and $\boldsymbol{\omega} \overset{\text{def}}{=} \boldsymbol{\omega}_{\mathrm{b/i}}$ is the angular rate of the spacecraft with respect to an inertial reference frame. Equation (3) connects the spacecraft's angular momentum with its angular rate, which is in turn connected to its attitude by the rotational kinematics:

(4) $$\dot{\underline{\boldsymbol{q}}} = \frac{1}{2}\underline{\boldsymbol{\omega}} \otimes \underline{\boldsymbol{q}}$$

In Eq. (4), $\underline{\boldsymbol{q}} \overset{\text{def}}{=} \underline{\boldsymbol{q}}_{\mathrm{bi}} = \begin{bmatrix} q_0 \\ \boldsymbol{q} \end{bmatrix}$ is a unit quaternion describing the spacecraft's attitude, $\underline{\boldsymbol{\omega}} \overset{\text{def}}{=} \begin{bmatrix} 0 \\ \boldsymbol{\omega} \end{bmatrix}$ is the quaternion notation of $\boldsymbol{\omega}$, and $\otimes$ denotes the quaternion multiplication as defined in [7].

A typical attitude control system architecture is shown in Figure 3. The guidance part generates a reference trajectory $\left\{\underline{\boldsymbol{q}}_{\mathrm{ref}}(t), \boldsymbol{\omega}_{\mathrm{ref}}(t)\right\}$ from observation targets, using specialized software such as e.g. ASSET [8]. The attitude controller computes the error between the commanded and the estimated attitude and rate of the satellite and commands a torque or angular momentum in order to correct the offset. This dynamic command is then mapped to a desired gimbal angle or gimbal rate by the CMG commanding (steering law). Both controller and commanding have to be specifically designed and tuned for each new mission and shall therefore be verified in simulations and hardware-in-the-loop experiments.

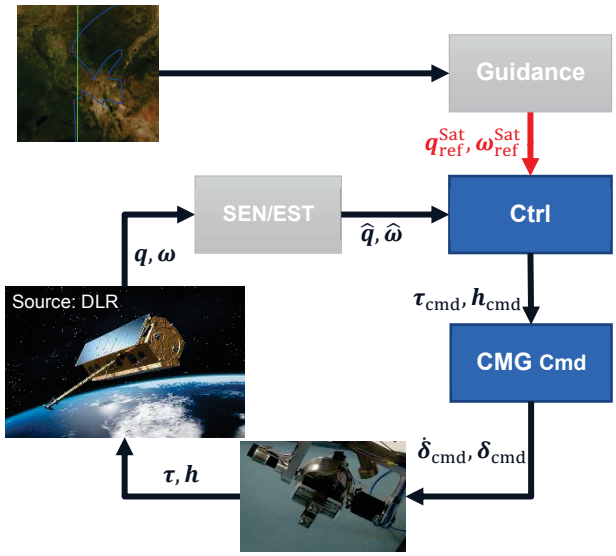

Figure 3 Attitude Control System Architecture

3. INTREPID HARDWARE DEMONSTRATOR

The INTREPID hardware demonstrator (see Figure 4) has been manufactured by Surrey Space Centre and was commissioned at the Airbus site in Immenstaad in 2015.

INTREPID is an air-bearing table with four CMG actuators that can rotate the table around all three axes. The CMGs can be mounted in two different array architectures (roof or pyramid) with an adjustable skew angle for both cases. In order to achieve a maximal mechanical decoupling, eight LiPo batteries provide enough power for experiments lasting up to one hour. The avionics consist of a real-time on-board computer, a high-accuracy inertial measurement unit (IMU), and an absolute attitude determination system based on infrared LEDs [9].

Even though INTREPID is fully equipped for the verification of attitude control algorithms, there are significant differences between the testbed and a satellite in Earth orbit:

1) INTREPID has a fixed center of rotation as opposed to a satellite which always rotates around its center of mass. Therefore, a mass balancing system consisting of four movable masses is used to shift the center of mass to the center of rotation.

2) An unconstrained rotation is only possible around the vertical axis; around the horizontal axes the mounting base imposes a tilt angle constraint of around 30°-40°.
3) There is no orbital motion, hence for a constant attitude the line of sight remains constant as well. Mathematically speaking, there is no rotation of the Nadir frame with respect to the inertial frame.

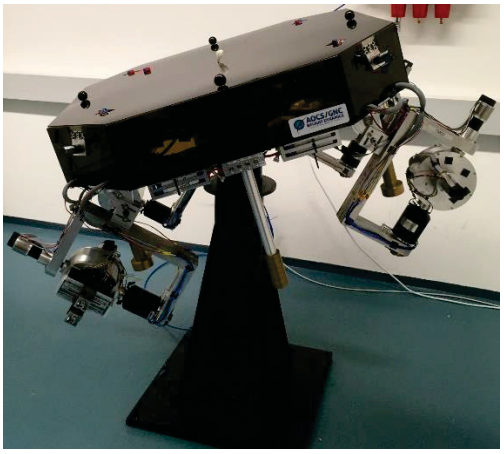

Figure 4 INTREPID Hardware Demonstrator

4. GENERAL SCALING ASPECTS

In the scope of AOCS algorithms, different control objectives have to be verified, of which we will briefly discuss the following:

1) Functionality/stability of attitude controller
2) Damping of flexible modes
3) Performance of attitude controller
4) Suitability of CMG steering law

The main challenge regarding the functionality of attitude control stems from the specific reference trajectory with fast slew maneuvers followed by observation phases with precision pointing requirements. The attitude controller has to follow the large-angle maneuver and then stabilize the spacecraft in the commanded final attitude at the correct time, otherwise the target cannot be observed. A suitable similarity condition is therefore the kinematic profile $\left\{\underline{\boldsymbol{q}}_{\mathrm{ref}}(t), \boldsymbol{\omega}_{\mathrm{ref}}(t)\right\}$ itself.

Whether flexible modes (such as solar arrays, large antennas, or propellant sloshing) are excited during a slew maneuver depends mainly on their eigenfrequencies and their proximity to the controller bandwidth. A similarity condition could therefore be the same eigenfrequency, maybe coupled with some “energy measure” relating the deflection of the mode shape function to some characteristic length of the spacecraft.

The (pointing) performance of the attitude control system is limited by the accuracy of sensors and actuators. Ground-based demonstrators rarely use flight hardware, hence a verification of an algorithm’s performance requires identifying the testbed’s noise sources and relating their noise characteristics to those of the sensors envisaged for the mission.

Finally, the CMG steering law maps a commanded angular momentum or torque to a gimbal angle or gimbal rate command, i.e., it inverts Eq. (1) or (2). As the angular momentum of each single CMG is a function of its gimbal angle, the main challenge to steering algorithms lies in unfavorable gimbal configurations, especially near or at the envelope. Therefore, a suitable similarity condition is to ensure the same load on the CMG array, which we will discuss in detail in the next section.

5. SCALING FOR STEERING VERIFICATION

5.1. Preliminaries

Consider the four-CMG roof array as shown in Figure 5, which consists of two CMG pairs acting in the *xy*- and *xz*'-plane, respectively.

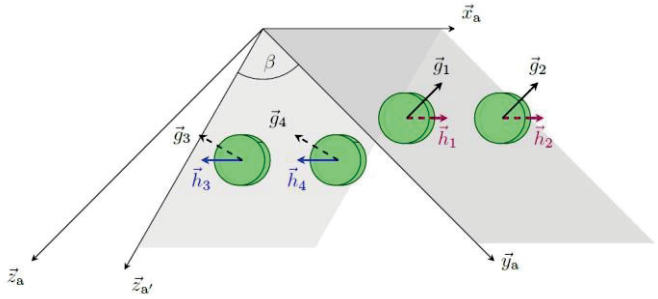

Figure 5 Four-CMG Roof Array

The skew angle β can be used as a design parameter to adjust the shape of the CMG array’s angular momentum envelope, i.e. the amount of angular momentum and torque that can be realized.

Defining the orthogonal array frame $\mathcal{A} = \{\boldsymbol{x}_{\mathrm{a}}, \boldsymbol{y}_{\mathrm{a}}, \boldsymbol{z}_{\mathrm{a}}\}$ and the skewed array frame $\mathcal{A}' = \{\boldsymbol{x}_{\mathrm{a}}, \boldsymbol{y}_{\mathrm{a}}, \boldsymbol{z}_{\mathrm{a}'}\}$ according to Figure 5, the CMG array’s angular momentum can be expressed in the two frames as ${}_{\mathrm{a}}\boldsymbol{h} = [h_x \quad h_y \quad h_z]^{\mathrm{T}}$ and ${}_{\mathrm{a}'}\boldsymbol{h} = [h_x \quad h_{y'} \quad h_{z'}]^{\mathrm{T}} = \boldsymbol{T}_{\mathrm{a}'\mathrm{a}}\ {}_{\mathrm{a}}\boldsymbol{h}$, where:

$$\boldsymbol{T}_{a'a} = \begin{bmatrix} 1 & 0 & 0 \\ 0 & 1 & -\cos\beta/\sin\beta \\ 0 & 0 & 1/\sin\beta \end{bmatrix}$$

$$\boldsymbol{T}_{\mathrm{aa}'} = \boldsymbol{T}_{\mathrm{a}'\mathrm{a}}^{-1} = \begin{bmatrix} 1 & 0 & 0 \\ 0 & 1 & \cos\beta \\ 0 & 0 & \sin\beta \end{bmatrix}$$

Note that as $\mathcal{A}'$ is not orthonormal, $\det \boldsymbol{T}_{\mathrm{a}'\mathrm{a}} = 1/\sin\beta$, hence in general $\boldsymbol{T}_{\mathrm{a}'\mathrm{a}}^{-1} \neq \boldsymbol{T}_{\mathrm{a}'\mathrm{a}}^{\mathrm{T}}$ and the Euclidean norm of a vector $\boldsymbol{h}$ expressed in the skewed frame has to be calculated using the metric tensor $\boldsymbol{T}_{\mathrm{aa}'}^{\mathrm{T}}\boldsymbol{T}_{\mathrm{aa}'}$:

$$\left\|{}_{\mathrm{a}'}\boldsymbol{h}\right\|_2 = \sqrt{{}_{\mathrm{a}'}\boldsymbol{h}^{\mathrm{T}}\,\boldsymbol{T}_{\mathrm{aa}'}^{\mathrm{T}}\boldsymbol{T}_{\mathrm{aa}'}\ {}_{\mathrm{a}'}\boldsymbol{h}} = \sqrt{h_x^2 + h_{y'}^2 + h_{z'}^2 + 2\cos\beta\ h_{y'}h_{z'}}$$

Using Eq. (3), we can now reformulate a kinematic reference trajectory $\{\underline{q}_{\mathrm{ref}}(t), \boldsymbol{\omega}_{\mathrm{ref}}(t)\}$ as a commanded angular momentum trajectory:

$$\boldsymbol{h} \stackrel{\text{def}}{=} \boldsymbol{h}_{\mathrm{cmd}} = \boldsymbol{H}_{\mathrm{tot}} - \boldsymbol{J}\boldsymbol{\omega}_{\mathrm{ref}} \tag{5}$$

5.2. Similarity Measure for CMG Array Utilization

For an orthogonal four-CMG roof array, [10] introduced the "angular momentum norm" that relates a given angular momentum command ${}_{\mathrm{a}}\boldsymbol{h} = [h_x \quad h_y \quad h_z]^{\mathrm{T}}$ to the maximum angular momentum in the same direction:

$$\|\boldsymbol{h}\|_H \stackrel{\text{def}}{=} \|\boldsymbol{h}\|_2 / H_{\max}(\boldsymbol{h}) = \begin{cases} \dfrac{\max\{|h_y|, |h_z|\}}{2h_{\mathrm{fw}}} & \text{if } h_x^2 \le |h_y^2 - h_z^2| \\ \dfrac{\sqrt{\left(h_x^2 + h_y^2 + h_z^2\right)^2 - 4h_y^2 h_z^2}}{4h_{\mathrm{fw}}|h_x|} & \text{if } h_x^2 > |h_y^2 - h_z^2| \end{cases} \tag{6}$$

Using the skewed array frame introduced above, we will now extend Eq. (6) to the general case ($\beta \neq \pi/2$) by repeating the derivation of [10]. Again, we start by finding the maximum angular momentum for a given angular momentum command:

$$\boldsymbol{H}_{\max}(\boldsymbol{h}) = \begin{bmatrix} H_x \\ H_{y'} \\ H_{z'} \end{bmatrix} = \clubsuit\boldsymbol{h} \tag{7}$$

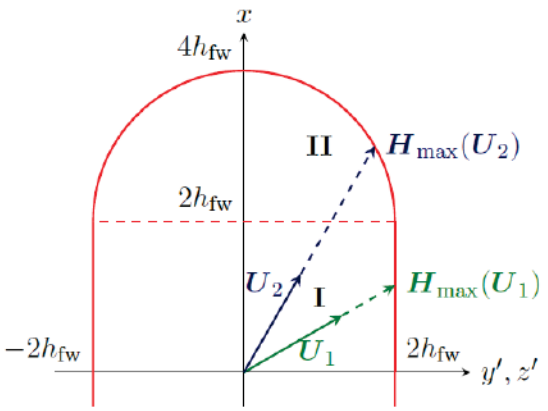

Figure 6 Momentum Envelope Projection on xy'/xz' Plane

Figure 6 shows the projection of the angular momentum envelope to the xy' and xz' planes. Note that the horizontal axis does not represent a physical axis in space, but corresponds to the coordinate values of the angular momentum expressed in the skewed frame $\mathcal{A}'$. Two main cases can be distinguished:

I. If $|H_x| \le 2h_{\mathrm{fw}}$, then $\boldsymbol{H}_{\max}$ lies on patch I
II. If $|H_x| > 2h_{\mathrm{fw}}$, then $\boldsymbol{H}_{\max}$ lies on patch II

According to Figure 7, case I can be distinguished further:

a. If $|H_x| \le 2h_{\mathrm{fw}}$ and $|h_{y'}| \ge |h_{z'}|$, then $\boldsymbol{H}_{\max}$ lies on patch Ia and $\clubsuit = 2h_{\mathrm{fw}}/|h_{y'}|$

b. If $|H_x| \le 2h_{\mathrm{fw}}$ and $|h_{y'}| < |h_{z'}|$, then $\boldsymbol{H}_{\max}$ lies on patch Ib and $\clubsuit = 2h_{\mathrm{fw}}/|h_{z'}|$

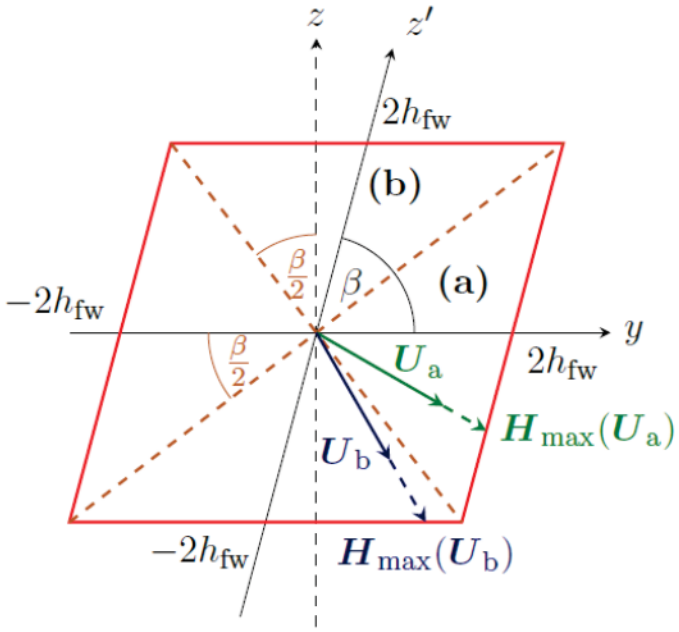

Figure 7 Momentum Envelope Projection on yz Plane

In case Ia, $\boldsymbol{H}_{\max} = [H_x \quad 2h_{\mathrm{fw}} \quad H_{z'}]^{\mathrm{T}}$, which is only possible if $\sqrt{H_x^2 + H_{z'}^2} \le 2h_{\mathrm{fw}}$, which using Eq. (7) yields:

$$h_x^2 \le h_{y'}^2 - h_{z'}^2, \tag{8}$$

Analogously, in case Ib, $\boldsymbol{H}_{\max} = [H_x \quad H_{y'} \quad 2h_{\mathrm{fw}}]^{\mathrm{T}}$, which is only possible for $\sqrt{H_x^2 + H_{y'}^2} \le 2h_{\mathrm{fw}}$ or:

$$h_x^2 \le h_{z'}^2 - h_{y'}^2, \tag{9}$$

As a result, $\boldsymbol{H}_{\max}$ lies on patch I if

$$h_x^2 \le |h_{y'}^2 - h_{z'}^2| \tag{10}$$

In case II, the angular momenta of both CMG pairs have to be maximized in order to reach $\boldsymbol{H}_{\max}$, which yields the following condition:

$$|H_x| = \clubsuit|h_x| = \sqrt{\left(2h_{fw}\right)^2 - \left(\kappa h_{y'}\right)^2} + \sqrt{\left(2h_{fw}\right)^2 - (\kappa h_{z'})^2} \tag{11}$$

Solving Eq. (11) for ♣ yields

$$\clubsuit = \begin{cases} \dfrac{2h_{\mathrm{fw}}}{\max\{|h_{y'}|, |h_{z'}|\}} & \text{if } h_x^2 \le \left|h_{y'}^2 - h_{z'}^2\right| \\ \dfrac{4h_{\mathrm{fw}}|h_x|}{\sqrt{\left(h_x^2 + h_{y'}^2 + h_{z'}^2\right)^2 - 4h_{y'}^2 h_{z'}^2}} & \text{if } h_x^2 > \left|h_{y'}^2 - h_{z'}^2\right| \end{cases} \tag{12}$$

From the definition of the angular momentum norm and Eq. (7) it follows immediately that:

$$\|\boldsymbol{h}\|_H = \|\boldsymbol{h}\|_2 / H_{\max}(\boldsymbol{h}) = \begin{cases} \dfrac{\max\{|h_{y'}|, |h_{z'}|\}}{2h_{\mathrm{fw}}} & \text{if } h_x^2 \le \left|h_{y'}^2 - h_{z'}^2\right| \\ \dfrac{\sqrt{\left(h_x^2 + h_{y'}^2 + h_{z'}^2\right)^2 - 4h_{y'}^2 h_{z'}^2}}{4h_{\mathrm{fw}}|h_x|} & \text{if } h_x^2 > \left|h_{y'}^2 - h_{z'}^2\right| \end{cases} \tag{13}$$

This result is identical in structure to the result in [10], but by using the skewed coordinates $h_{y'}$ and $h_{z'}$ it is valid for arbitrary skew angles. Equation (13) maps a 3D angular momentum command to a scalar, hence we need to recover the directional information by defining the "envelope utilization"

$$\boldsymbol{u}_h \stackrel{\text{def}}{=} \|\boldsymbol{h}\|_H \boldsymbol{d}_h, \tag{14}$$

where $\boldsymbol{d}_h \stackrel{\text{def}}{=} \boldsymbol{h}/\|\boldsymbol{h}\|_2$ denotes the direction of the angular momentum command $\boldsymbol{h}$.

5.3. Scaling Law

With the definition of the envelope utilization, we can now formulate the scaling objective mathematically: Two profiles $\boldsymbol{h}^{\mathrm{Sat}}(t)$ and $\boldsymbol{h}^{\mathrm{Int}}(t)$ are similar if their envelope utilizations are equal:

$$\boldsymbol{u}_h^{\mathrm{Sat}}(t) = \boldsymbol{u}_h^{\mathrm{Int}}(t) \tag{15}$$

Eq. (14) is expressed in the skewed array frame, whereas reference trajectories are typically given in the body frame. Therefore, the complete scaling law is obtained by inserting Eqs. (13) and (14) into Eq. (15) and transforming both sides into their respective body frames:

$${}_{\mathrm{b}}\boldsymbol{h}^{\mathrm{Int}}(t) = \frac{h_{\mathrm{fw}}^{\mathrm{Int}}}{h_{\mathrm{fw}}^{\mathrm{Sat}}} \boldsymbol{T}_{\mathrm{ba}}^{\mathrm{Int}} \boldsymbol{T}_{\mathrm{aa'}}^{\mathrm{Int}} \boldsymbol{T}_{\mathrm{a'a}}^{\mathrm{Sat}} \boldsymbol{T}_{\mathrm{ab}}^{\mathrm{Sat}} {}_{\mathrm{b}}\boldsymbol{h}^{\mathrm{Sat}}(t) \tag{16}$$

Differentiating Eq. (16) with respect to time and inserting Eq. (2) yields:

$${}_{\mathrm{b}}\boldsymbol{C}^{\mathrm{Int}} \dot{\boldsymbol{\delta}}^{\mathrm{Int}} = \frac{h_{\mathrm{fw}}^{\mathrm{Int}}}{h_{\mathrm{fw}}^{\mathrm{Sat}}} \boldsymbol{T}_{\mathrm{ba}}^{\mathrm{Int}} \boldsymbol{T}_{\mathrm{aa'}}^{\mathrm{Int}} \boldsymbol{T}_{\mathrm{a'a}}^{\mathrm{Sat}} \boldsymbol{T}_{\mathrm{ab}}^{\mathrm{Sat}} {}_{\mathrm{b}}\boldsymbol{C}^{\mathrm{Sat}} \dot{\boldsymbol{\delta}}^{\mathrm{Sat}} \tag{17}$$

Define the normalized Jacobian $\overline{\boldsymbol{C}} \stackrel{\text{def}}{=} 1/h_{\mathrm{fw}} \boldsymbol{C}$ and express Eq. (17) in the skewed array frame:

$${}_{\mathrm{a'}}\overline{\boldsymbol{C}}^{\mathrm{Int}}(\boldsymbol{\delta}^{\mathrm{Int}}) \dot{\boldsymbol{\delta}}^{\mathrm{Int}} = {}_{\mathrm{a'}}\overline{\boldsymbol{C}}^{\mathrm{Sat}}(\boldsymbol{\delta}^{\mathrm{Sat}}) \dot{\boldsymbol{\delta}}^{\mathrm{Sat}} \tag{18}$$

For $\boldsymbol{\delta}^{\mathrm{Int}} = \boldsymbol{\delta}^{\mathrm{Sat}}$, the normalized Jacobians are identical, hence commanding identical gimbal rates will result in a similar torque and thus angular momentum profile.

Using Eq. (5), we can compute the scaled angular rate command profile to:

$${}_{\mathrm{b}}\boldsymbol{\omega}_{\mathrm{b/i}}^{\mathrm{Int}}(t) = \frac{h_{\mathrm{fw}}^{\mathrm{Int}}}{h_{\mathrm{fw}}^{\mathrm{Sat}}} \boldsymbol{J}_{\mathrm{Int}}^{-1} \boldsymbol{T}_{\mathrm{ba}}^{\mathrm{Int}} \boldsymbol{T}_{\mathrm{aa'}}^{\mathrm{Int}} \boldsymbol{T}_{\mathrm{a'a}}^{\mathrm{Sat}} \boldsymbol{T}_{\mathrm{ab}}^{\mathrm{Sat}} \boldsymbol{J}_{\mathrm{Sat}} {}_{\mathrm{b}}\boldsymbol{\omega}_{\mathrm{b/N}}^{\mathrm{Sat}}(t) \tag{19}$$

Finally, the attitude command profile can be obtained by numerical integration of the rotational kinematics (4).

5.4. Compliance with Testbed Limits

In the scaling law of Eq. (19), the scaled angular rate command is proportional to the angular momentum of the testbed's CMG flywheels, which has not yet been fixed. As a result, we can tune this parameter in order to ensure compliance with testbed limitations such as:

1) Gimbal motor constraints
2) Attitude constraints

A simplified model for the gimbal dynamics [5] is

$$J_{\mathrm{gfw}} \ddot{\delta} = \tau_{\mathrm{g}} + J_{\mathrm{fw}} \Omega_{\mathrm{fw}} \boldsymbol{\omega}^{\mathrm{T}} \boldsymbol{o}(\delta), \tag{20}$$

where τ_{g} is the gimbal motor torque, J_{fw} is the moment of inertia of the flywheel, J_{gfw} is the moment of inertia of the gimbal/flywheel assembly, Ω_{fw} is the flywheel spin rate, and $\boldsymbol{o} = \boldsymbol{c}/\|\boldsymbol{c}\|$ is the current direction of the CMG's output torque. The CMG gimbal motor has to accelerate the gimbal while compensating any disturbances, hence the maximum gimbal motor torque can be split into

$$\tau_{\mathrm{g,max}} = J_{\mathrm{gfw}} \ddot{\delta}_{\max} + \tau_{\mathrm{hold}}$$

with a desired maximum gimbal acceleration $\ddot{\delta}_{\max}$ and a holding torque τ_{hold} to compensate disturbances. From Eq. (20), the holding torque has to compensate the term $\boldsymbol{\omega}^{\mathrm{T}} \boldsymbol{c}$, hence reformulating yields an upper limit for the angular rate:

$$\omega_{\max} = \frac{\tau_{\mathrm{g,max}} - J_{\mathrm{gfw}} \ddot{\delta}_{\max}}{J_{\mathrm{fw}} \Omega_{\mathrm{fw}}}$$

For INTREPID, $\tau_{\mathrm{g,max}} = 4.23\ \mathrm{Nm}$, $J_{\mathrm{gfw}} = 0.04\ \mathrm{kgm^2}$, and $J_{\mathrm{fw}} = 0.01\ \mathrm{kgm^2}$. For a desired $\ddot{\delta}_{\max} \approx 3.5\ \mathrm{rad/s^2}$, the testbed's angular rate limits for varying flywheel spin rates are shown in Table 1. Due to the conservative design of the gimbal motors, their constraints will be satisfied for any reasonable experiment.

Table 1 INTREPID Gimbal Constraints

Spin Rate [rpm]	Max. angular rate [deg/s]
1000	223.79
2300	97.30
6000	37.30

INTREPID's attitude constraint is a tilt angle constraint: The lower part of the CMG assemblies would hit the cen-

ter base if the body frame's *z*-axis deflected too much from the vertical direction, hence taking advantage of the kinematic relationship $\boldsymbol{T}_{\mathrm{bi}} = (q_0^2 - \boldsymbol{q}^{\mathrm{T}}\boldsymbol{q})\boldsymbol{I} + 2\boldsymbol{q}\boldsymbol{q}^{\mathrm{T}} - 2q_0\boldsymbol{q}^{\times}$ [7], the tilt angle is defined as:

$$\alpha \stackrel{\mathrm{def}}{=} \arccos\left({}_{\mathrm{i}}\boldsymbol{z}_{\mathrm{i}}^{\mathrm{T}}\boldsymbol{T}_{\mathrm{ib}}\,{}_{\mathrm{b}}\boldsymbol{z}_{\mathrm{b}}\right) = \arccos\left(1 - 2(q_1^2 + q_2^2)\right) \tag{21}$$

After choosing an initial CMG flywheel angular momentum $h_{\mathrm{fw},0}^{\mathrm{INT}}$, the scaled attitude profile can be evaluated against the tilt angle:

$$m \stackrel{\mathrm{def}}{=} \max_t \alpha(t) \Big/ \alpha_{\max}$$

If $m > 1$, then $h_{\mathrm{fw}}^{\mathrm{INT}}$ has to be suitably reduced until the scaled attitude profile satisfies the tilt angle constraint.

6. SIMULATION RESULTS

For the verification of the proposed scaling law, a hypothetical agile satellite mission is modeled with the parameters shown in Table 2.

Table 2 Case Study Parameters

	Spacecraft	INTREPID
$\boldsymbol{J}$ [kgm²]	$\begin{bmatrix} 2500 & & \\ & 10000 & \\ & & 10000 \end{bmatrix}$	$\begin{bmatrix} 26.2 & -1.76 & -1.38 \\ -1.76 & 25.2 & 0.93 \\ -1.38 & 0.93 & 35.1 \end{bmatrix}$
β [deg]	70	90
h_{fw} [Nms]	90	3.14, 0.09
$\boldsymbol{T}_{\mathrm{ab}}$ [-]	$\boldsymbol{T}_3\left(\frac{\pi}{2}\right)$	$\boldsymbol{T}_1\left(\frac{5\pi}{4}\right)\boldsymbol{T}_3\left(-\frac{\pi}{4}\right)$
δ_0 [rad]	$\left[-\frac{\pi}{3}, \frac{\pi}{3}, -\frac{\pi}{3}, \frac{\pi}{3}\right]$	

The commanded angular rate profile and the corresponding CMG angular momentum command are shown in Figure 8 and Figure 9, respectively.

The first scaling is performed for a CMG flywheel rate of 3000 rpm ($h_{\mathrm{fw}} = 3.14\ \mathrm{Nms}$), yielding the angular rate and angular momentum command profiles shown in Figure 10 and Figure 11. As $m \gg 1$ for this scenario, the CMG flywheel spin rate is reduced to 90 rpm ($h_{\mathrm{fw}} \approx 0.09\mathrm{Nms}$) which satisfies the tilt angle constraint. The corresponding angular rate and angular momentum command profiles are shown in Figure 12 and Figure 13.

As illustrated by Figure 9, Figure 11, and Figure 13, the angular momentum profiles in all three scenarios have the same utilization of the respective angular momentum envelopes. To verify this expectation, we set the initial gimbal angles to those of Table 2 and compute a gimbal rate command profile using the Moore-Penrose pseudoinverse steering law to invert Eq. (2):

$$\dot{\boldsymbol{\delta}} = \boldsymbol{C}^{\mathrm{T}}(\boldsymbol{C}\boldsymbol{C}^{\mathrm{T}})^{-1}\dot{\boldsymbol{h}}_{\mathrm{cmd}}$$

As shown in Figure 14 for the xy pair and Figure 15 for the xz' pair, the resulting gimbal angle profiles coincide for all three cases. Of particular interest is the time interval between 890 s and 935 s, where the xz' pair encounters a singularity as both CMGs are aligned parallel to each other. As such a singularity constitutes a loss of controllability around an axis, these configurations are to be avoided in practice, if possible by using a more suitable steering law [6]. For this study, the choice of the Moore-Penrose steering law was intentional as it is most likely to exhibit singularity-related issues. The fact that this challenge for a steering algorithm appears in both scaled scenarios justifies the scaling method as a means for the verification of steering algorithms.

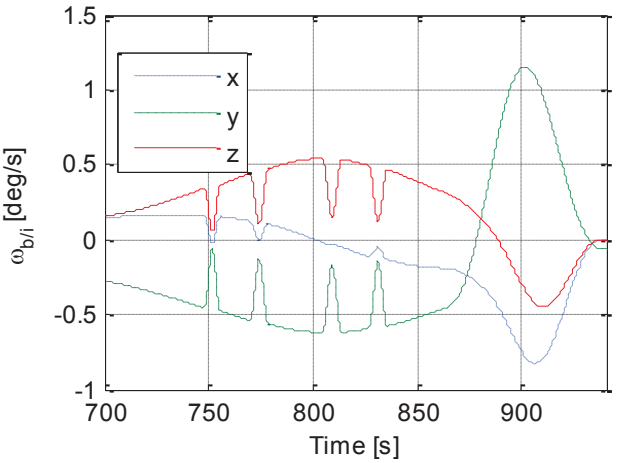

Figure 8 Spacecraft Angular Rate Command

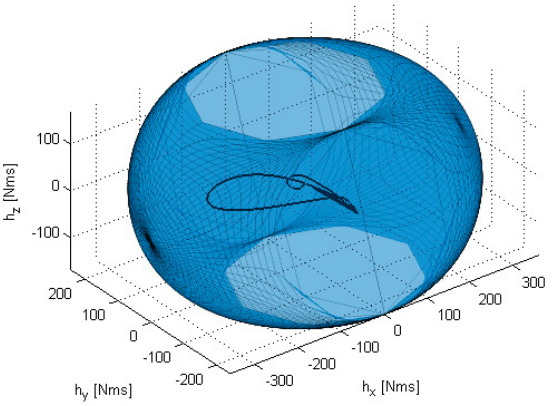

Figure 9 CMG Angular Momentum Spacecraft

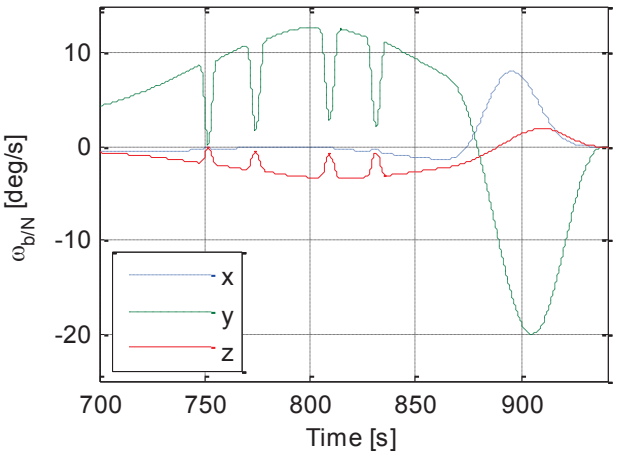

Figure 10 Angular Rate Command INTREPID (3.14 Nms)

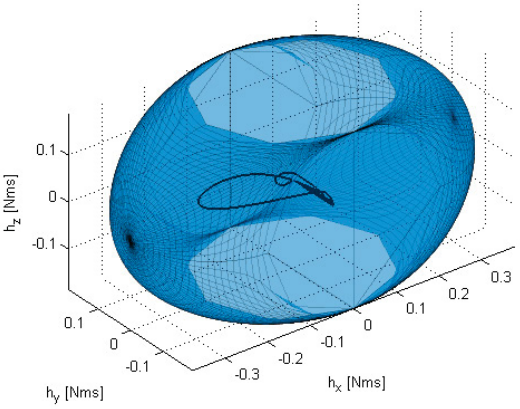

Figure 13 Angular Momentum INTREPID (h_{fw} = 0.09 Nms)

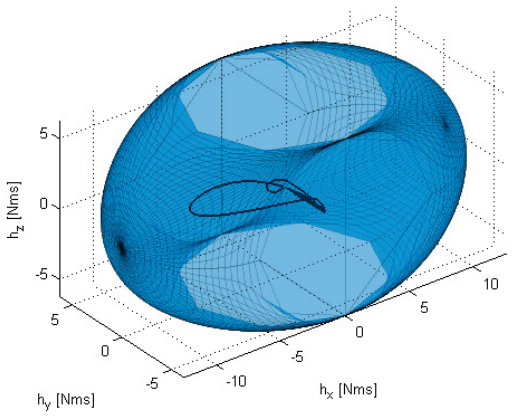

Figure 11 Angular Momentum INTREPID (h_{fw} = 3.14 Nms)

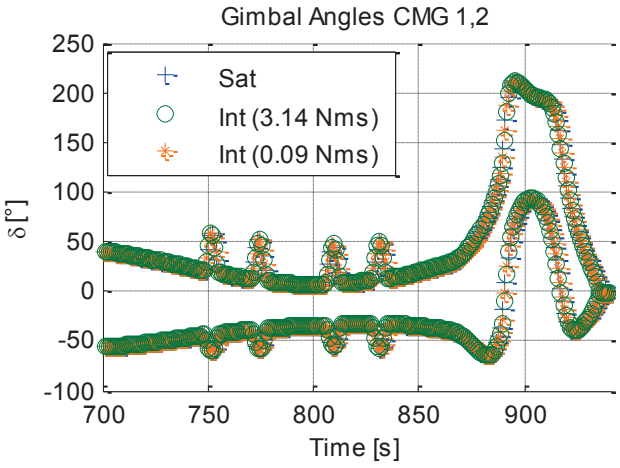

Figure 14 Gimbal Angle Profiles CMGs 1 and 2

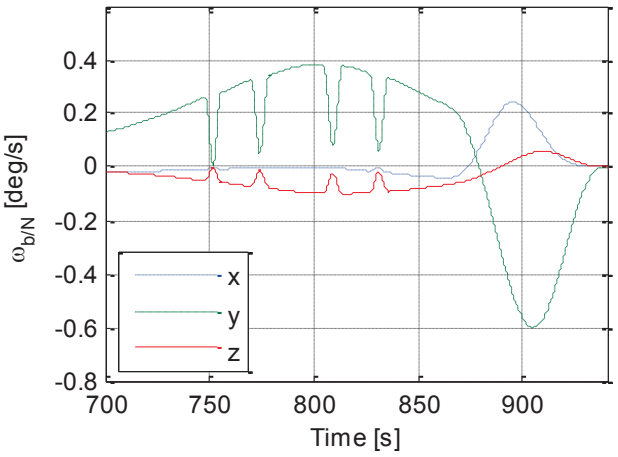

Figure 12 Angular Rate Command INTREPID (0.09 Nms)

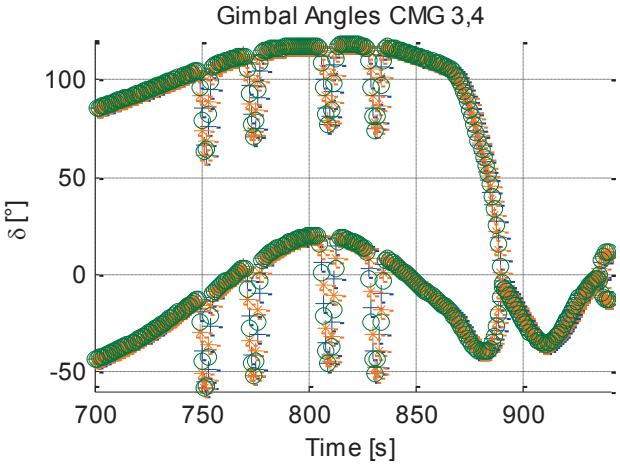

Figure 15 Gimbal Angle Profiles CMGs 3 and 4

7. CONCLUSIONS

The experimental verification of AOCS algorithms requires representative test definitions depending on the envisaged mission, the dynamical and geometric properties of the testbed, and the part of the algorithms that are to be verified. In this paper, some similarity criteria are proposed for different components of AOCS algorithms and the angular momentum envelope utilization is identified as the critical quantity for the verification of CMG steering laws.

With the proposed envelope utilization scaling method, it is possible to verify steering algorithms for CMG roof-arrays with arbitrary moments of inertia, flywheel angular momenta, array orientations, and skew angles. Retaining the same envelope utilization ensures that the steering task encounters similar challenges posed by e.g. singular states.

Future work on this topic may pick up on the similarity conditions outlined in section 4 such as a rigorous derivation of an “energy measure” for flexible modes and/or an investigation on the scaling of noise contributors.

ACKNOWLEDGMENTS

This work has been financially supported by the Space Agency of the German Aerospace Center (DLR, Deutsches Zentrum für Luft- und Raumfahrt e.V.) with means of the Federal Ministry for Economic Affairs and Energy under support number 50 RR 1702.

REFERENCES

[1] M. A. Gleyzes, L. Perret and P. Kubik, "Pleiades System Architecture and Main Performances," in *International Archives of the Photogrammetry, Remote Sensing and Spatial Information Sciences*, 2012.

[2] G. Margulies and J. N. Aubrun, "Geometric theory of single-gimbal control moment gyro systems," *Journal of the Astronautical Sciences,* vol. 26, no. 2, pp. 159-191, 1978.

[3] A. Kornienko, T. Ott, J. Rieber, J. Levenhagen, R. Geshnizjani and W. Fichter, "Advanced AOCS/GNC Technology Demonstration using Experimental Testbed," in *10th International ESA Conference on Guidance, Navigation & Control Systems*, Salzburg, 2017.

[4] R. Geshnizjani, A. Kornienko, J. Levenhagen and W. Fichter, "INTREPID: A Ground-Based CMG Hardware Demonstrator for Agile Satellite Attitude Control Design," in *66. Deutscher Luft- und Raumfahrtkongress*, München, 2017.

[5] F. A. Leve, B. J. Hamilton and M. A. Peck, Spacecraft Momentum Control Systems, Springer International Publishing, 2015.

[6] H. Kurokawa, "Survey of theory and steering laws of single-gimbal control moment gyros," *Journal of Guidance, Control, and Dynamics,* vol. 30, no. 5, pp. 1331-1340, 2007.

[7] M. D. Shuster, "A Survey of Attitude Representation," *The Journal of the Astronautical Sciences,* vol. 41, no. 4, pp. 439-517, 1993.

[8] M. F. Barschke, J. Levenhagen, D. Reggio and P. C. E. Roberts, "ASSET: a software tool for the evaluation of manoeuvre capabilities of highly agile satellites," *CEAS Space Journal,* vol. 6, pp. 37-45, 2014.

[9] D. C. Bamber, J. L. Forshaw, T. E. Frame, G. Aglietti, R. Geshnizjani, S. Görries, A. Kornienko, J. Levenhagen, Y. Gao and A. Chanik, "Absolute attitude determination system for a spherical air bearing testbed," in *66th International Astronautical Congress*, Jerusalem, 2015.

[10] D. Verbin and V. Lappas, "Rapid rotational maneuvering of rigid satellites with hybrid actuators configuration," *Journal of Guidance, Control, and Dynamics,* vol. 36, no. 2, pp. 532-547, 2013.